Engineered Science
DOI: https://dx.doi.org/10.30919/es1055

Non-Linear Transient Analysis of Three Lobe Bearing Functioning through Pseudo-plastic Lubricant with Slip/No-slip Conditions

Amar Murthy A,[1] Raghunandana. K,[1,*] Jamaluddin Hindi,[1,*] Muralishwara K[1] and Kasirajan Kasipandian[2]

Abstract

The study examines the combined impact of wall slip and pseudoplastic fluid on bearing system stability using a non-linear transient technique. The pseudoplastic effect is fused using the power law model, and the influence of slip lengths on lubricating surfaces is examined using the Navier slip condition. MATLAB code is utilized to solve the Reynolds equation using the finite-difference method and the Gauss-Seidel iterative method. By utilizing non-linear transient analysis, the journal center trajectories, which play a crucial role in determining the stability of the system, are estimated. The results of the investigation show that there is an approximate 21% improvement in the three-lobe bearing stability.

Keywords: Film thickness; Multilobe bearing; Nonlinear transient analysis; Non-Newtonian fluid; Wall-slip, power law index (PLI).
Received: 16 November 2023; Revised: 09 December 2023; Accepted: 09 December 2023.
Article type: Research article.

1. Introduction

To improve the performance qualities, such as a reduction in wear and friction, Newtonian fluid is blended with a variety of additives. The fluid exhibits non-Newtonian behavior when the shear stress and shear strain rates are nonlinear. The performance of the bearing is predicted with more realism and accuracy when the lubricant non-linearity behavior is considered. Enhanced manufacturing technology in recent times has enabled the attainment of extremely smooth surfaces. This method may be used, for example, on sliding surfaces, where it is useful in lowering friction and, consequently, wall slip between the solid-lubricant contact. Many studies have discovered that the commonly accepted 'no-slip' boundary condition is no longer relevant to most designed surfaces, since fluid flows against the non-wettable surface, causing wall slip at the liquid-solid interface. Also, it is found that[1,2] slip occurs on smooth surfaces due to weaker links between the solid and the lubricant surfaces. Friction force reduction between sliding surfaces has been demonstrated[3,4] thus enhancing component life and lowering energy usage. Better tribological performance can be attained by effectively using slip surfaces. Transient nonlinear analysis was used by Ren Lin *et al*.[5] to examine the non-Newtonian effect on the non-linear stability boundary of short journal bearings. Kane *et al*.[6] established a revised homogenized Reynolds equation of the Maxwell type for non-Newtonian lubricant, considering the effect of roughness of the surface. It was found that the obtained pressures by this averaging method compared with that of the direct heuristic method are very close. Aiumpornsin *et al*.[7] carried out a numerical analysis to determine the properties of elastic deformation and roughness of the surface of a bearing liner on both dynamic and static characteristics of elastohydrodynamic bearings operating with non-Newtonian fluid. Chiang *et al*.[8] based on Christensen's Stokes theory and stochastic model, predicted the effects of one-dimensional rough surface considered in longitudinal and transverse directions along with couple stress fluid on the linear stability speed threshold of hydrodynamic bearing.

According to Khonsari and Brewe,[9] micropolar lubricated bearings outperformed Newtonian lubricated bearings in

[1] *Department of Mechanical and Industrial Engineering, Manipal Institute of Technology, Manipal Academy of Higher Education, Manipal, Karnataka, 576104, India.*
[2] *Faculty of Engineering Built Environment and IT, MAHSA University, Bandar Saujana Putra, Selangor, 42610, Malaysia.*
**Email:* jamaluddin.hindi@manipal.edu (J. Hindi); raghu.bhat@manipal.edu (R. Bhat)

terms of friction reduction and load-carrying capacity. In the circumstance of pseudo-plastic fluids, Nessil *et al*.[10] quantitatively showed that the temperature, pressure, frictional force, and load-bearing capacity increased. Furthermore, dilatant lubricants improve load-carrying performance when compared to merely viscous fluids. The PLI had a stronger impact at larger ratios of eccentricity and the effects, according to Safar[11] experiments of a non-Newtonian fluid in an indefinitely long bearing. In their study of the performance characteristics of two lobe bearings using non-Newtonian-behaving lubricants, Rahmani *et al*.[12] showed that the power-law model is the best option. According to Crosby and Chetti,[13] the couple stress fluid element has a considerable impact on bearing performance when compared to Newtonian fluids, leading to enhanced stability. Using hydrodynamic journal bearings that were continuously under a single-direction responsive load, Researchers Majumdar and Raghunandana[14] researched the stability of lubricating fluids that function as non-Newtonian fluids. Chetti *et al*.[15] deliberated the effects of additive-enhanced lubricant and preload on a 3-lobed bearing. A high PLI non-Newtonian fluid was shown to enhance stability while lubricating a multilobe bearing, as per Das and Roy's[16] experiment.

Wall-slip is a crucial aspect that must be considered in addition to the non-Newtonian case. Ignoring it could lead to incomplete or inaccurate conclusions. Rao *et al*.[17] theoretically evaluated the effect of partial slip and textured surface of a journal and slider bearing. The impact of wall slip on bearing performance for a 2D finite span bearing was investigated by Ma *et al*.[18]

The impact of wall slide over the power loss and load-carrying capacity in hydrodynamic fluid film bearings was investigated using a finite element analysis by Aurelian *et al*..[19] An analysis was carried out by Chen *et al*.[20] to study the performance characteristics of a journal bearing considering an anisotropic slip.

Fortier *et al*.[21] examined the influence of a designed slip or no-slip surface on the performance of journal bearings. The effect of slip wedge surface was studied by Guo *et al*.[22] in slider and convergent gap of a journal bearing. Lin *et al*.[23] conducted a numerical study on shear flow in a sliding bearing with a partial slip surface to emphasize the effects of slip on sliding bearing characteristics such as friction force and load-carrying capacity. The tribological performances are different and more significant compared to the classical no-slip condition.[24-30] According to Lin *et al*.[31] research, journal bearing is impacted by slip area and its location. In their investigations, Mohseni *et al*.[32-34] have examined the impact of wall slip on convective heat transfer across different flow channel configurations.

Thus, the review reveals that prior research has explored the effects of the so-called "non-Newtonian effect" and the "slip effect" separately, and to a lesser extent, their combined effects, but solely concerning simple journal bearings.

The prime objective of this study is to assess the stability of the three-lobe bearing. To achieve this, a comprehensive mathematical model has been created using the Reynolds equation. This model considers both wall-slip effects and the nonlinear behavior of non-Newtonian fluid simultaneously. Through a non-linear transient analysis, the dynamic performance of a three-lobe bearing can be accurately predicted. MATLAB code is utilized to obtain a range of journal trajectories, which are then employed in an examination of the bearing's stability characteristics.

Potential real-world applications or industries where the findings might be applied

Advancements in manufacturing technology have paved the way for significant developments in various industries, enabling the achievement of high surface finish on bearing surfaces. This breakthrough has had a profound impact across sectors ranging from aerospace to automotive, medical appliances to construction materials. The potential for product miniaturization and customization has expanded as a result. These polished surfaces, resembling mirrors, have found application on sliding surfaces to effectively reduce friction, especially in solid-lubricant contacts. The utilization of such mirrored finish surfaces on sliding surfaces has been identified as one of the contributing factors to the mitigation of wall slip between solid-lubricant contacts, thereby enhancing friction reduction.

The incorporation of additives into lubricants can lead to non-linear behavior, which means that the performance of the lubricant does not follow a linear pattern with the amount of additive added. This non-linear behavior is extremely advantageous in the development of high-performance fluids for various applications. Manufacturers can carefully select and incorporate additives into lubricants to tailor their properties according to specific requirements and optimize their performance under different operating conditions.

For instance, in automotive applications, additives can be utilized to enhance the lubricant's ability to withstand high temperatures and pressures, reduce friction and wear, improve fuel efficiency, and extend the lifespan of engine components. In industrial applications, such as manufacturing and heavy machinery, additives can be employed to increase the lubricant's load-carrying capacity, minimize friction and wear in extreme operating conditions, and provide protection

against corrosion and oxidation. Non-linear behavior enables the formulation of lubricants that can endure heavy loads and extreme temperatures, guaranteeing smooth operation and prolonging equipment lifespan.

Moreover, non-linear behavior also offers advantages in specialty applications like aerospace, marine, and military. Additives can be used to enhance the lubricant's resistance to extreme temperatures, pressures, and environmental conditions, as well as provide specific properties such as anti-foaming, anti-rust, or anti-wear capabilities. Non-linear behavior allows for the customization of lubricants to meet the unique demands of these applications.

2. Methodology

2.1 Three-lobe bearing geometry

A journal bearing with three lobes has an ellipticity ratio (d) that is shifted from the center of the bearing. This design results in a tighter clearance between the shaft and the bearing, reducing friction and allowing for smoother rotation. The three lobes also provide additional stability to the shaft, making this type of bearing ideal for high-speed and high-load applications. Fig. 1 depicts the three-lobe journal-bearing geometry with the employed coordinate system. Each lobe L1, L2, and L3 subtends an angle of 120 degrees at the bearing's center O_b. During operation, the axis of the journal is eccentric (e) relative to the axis of the bearing. The radius of the journal is R and the radius of each lobe is R+C which includes the minor clearance and the ellipticity value of the preload factor. Due to the preload effect in the three lobe bearings, each lobe has a unique eccentricity ratio ε_L, ε_B, and ε_R and corresponding attitude angles ϕ_L, ϕ_B, and ϕ_R at any given moment and are given from Eq. (1) to Eq. (6).

For the left side lobe, eccentricity ratio, ε_L and attitude angle, ϕ_L are given by Eq. (1) and Eq. (2), respectively.

$$\varepsilon_L = \sqrt{\varepsilon^2 + \delta^2 - 2\varepsilon\delta\cos\left(\frac{\pi}{3} - \phi\right)} \tag{1}$$

$$\phi_L = sin^{-1}\left(\frac{\varepsilon\, sin\left(\frac{\pi}{3} - \phi\right)}{\varepsilon_L}\right) \tag{2}$$

For the bottom lobe, eccentricity ε_B and attitude angle, ϕ_B are given by Eq. (3) and Eq. (4), respectively.

$$\varepsilon_B = \sqrt{\varepsilon^2 + \delta^2 + 2\varepsilon\delta\, cos\,\phi} \tag{3}$$

$$\phi_B = sin^{-1}\left(\frac{\varepsilon\, sin\,\phi}{\varepsilon_B}\right) \tag{4}$$

For the right side lobe, eccentricity, ε_R and attitude angle, ϕ_R are given by Eq. (5) and Eq. (6), respectively.

$$\varepsilon_R = \sqrt{\varepsilon^2 + \delta^2 - 2\varepsilon\delta\cos\left(\frac{\pi}{3} + \phi\right)} \tag{5}$$

$$\phi_R = \frac{2\pi}{3} - sin^{-1}\left(\frac{\varepsilon\, sin\left(\frac{\pi}{3} + \phi\right)}{\varepsilon_R}\right) \tag{6}$$

The thickness of the film in the nth lobe of a three-lobe bearing can be calculated using Eq. (7).

$$h = C + e_p cos\left(\theta - \phi_p\right) \tag{7}$$

For the current work, the Navier slip model, $U_s = b.\left(\frac{\partial u}{\partial y}\right)$ is used. The model of slip length used in the present work is depicted in Fig. 2. The Navier slip model is based on the concept of slip velocity, which refers to the difference in velocity between the lubricant and the solid surface. By considering the Navier slip model we can arrive at the standard Reynolds equation (without slip) by assigning the values for B_{1x}, B_{2x}, B_{1y}, B_{2y} to zero. This feature is not available in any other models like the slip length model, limiting shear stress slip model, and slip intensity model. This helps us in validating the results by considering slip with the standard Reynolds

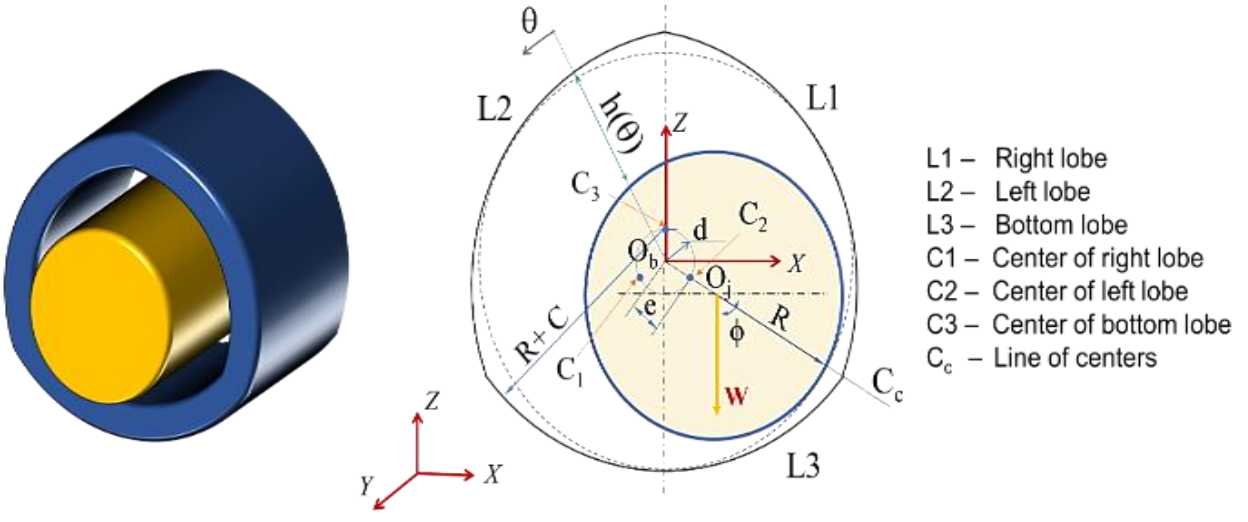

Fig. 1 Three lobe bearing pictorial view and geometry.

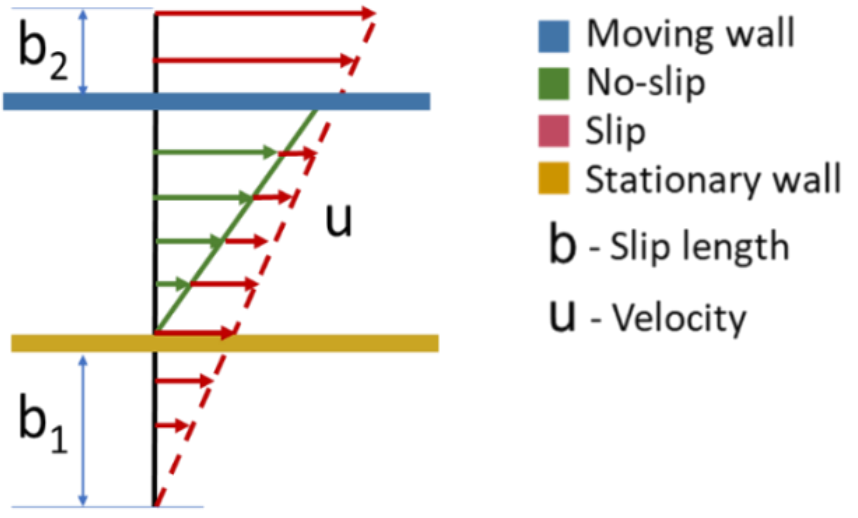

Fig. 2 Slip length model.

equation without slip. Moreover, the Navier slip model provides at most accurate results with less computation.

2.2 Boundary conditions

The chosen boundary conditions define the flow characteristics of a fluid close to a solid boundary and are based on the Reynolds boundary condition. These parameters are crucial in defining the general behavior of the fluid flow because they account for the pressure and velocity gradients at the boundary.

$\bar{P} = 0$ at extreme edges along the y-axis, *i.e.*, at $\bar{y}$=1 and $\bar{y}$=0

$\bar{P} = 0$ at θ =2π and θ =0.

With the fluid film's start and cavitation points are denoted by θ_s and θ_c, $\bar{P} = \left(\frac{\partial \bar{P}}{\partial \theta}\right)_{\theta_s<\theta<\theta_c} = 0$.

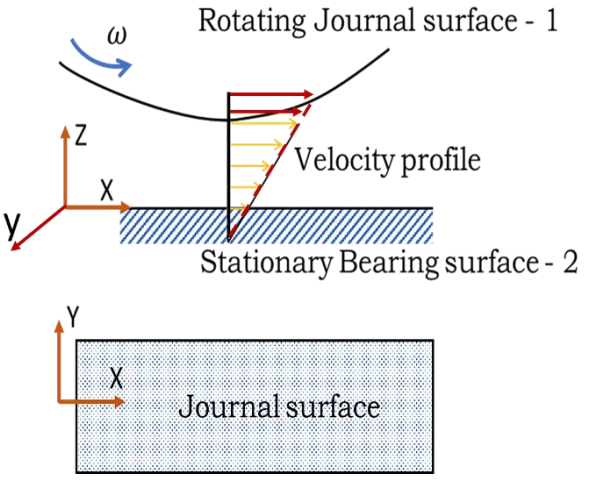

Fig. 3 Stationary and rotating surfaces of the bearing.

2.3 Developed mathematical model

The objective of this research is to investigate the influence of wall slip and non-Newtonian lubricant on the stability of multilobe bearings. This will be achieved by formulating a novel model or equation that builds upon the existing Reynolds equation. The study will specifically address two factors that have been overlooked in the Reynolds equation: the non-Newtonian behavior of the lubricant and the effect of wall slip on the sliding surfaces. The modified Reynolds equation is obtained by incorporating these factors, using momentum equations as the basis, and referring to the model created by Chen *et al.*[20] starting from the momentum equations. The present work is a continuation of our recently published research work.[35-37] The coordinate system and the surfaces used in deriving the equation are portrayed in Fig. 3. Pseudoplastic fluids are characterized by a reduction in viscosity as the shear rate increases. This model offers a straightforward and convenient approach to understanding and predicting the flow behavior of these fluids under various conditions. Moreover, the power law model enables easy comparison and analysis of different pseudoplastic fluids, thereby facilitating the development and optimization of processes involving such fluids. By incorporating the shear-thinning behavior, the power law model[35] expresses viscosity as a function of the shear rate. This relationship is represented by Eq. (8).

$$\mu = m\left(\frac{U}{h}\right)^{n-1} \tag{8}$$

A lower value of n signifies a more pronounced shear-thinning behavior, while a value of n close to 1 indicates that the fluid behaves more similarly to a Newtonian fluid.

Eqs. (9) and (10) describe the final forms of the proposed revised Reynolds equation in dimensional and nondimensional forms, respectively, for the two-dimensional flow of a non-Newtonian lubricant under the condition of

wall-slip.

$$\frac{\partial}{\partial x}\left[\left\{\frac{h}{2}\left[2u_{1x}+\frac{v_x}{h+b_{1x}+b_{2x}}(2b_{1x}+h)\right]-\frac{h^3}{12n\mu_0}\frac{\partial p}{\partial x}\left[\frac{3}{h}\frac{(2b_{1x}+h)(2b_{2x}+h)}{b_{1x}+h+b_{2x}}-2\right]\right\}\right]+\frac{\partial}{\partial y}\left\{\frac{h}{2}\left[2v_{1y}+\frac{v_y}{h+b_{1y}+b_{2y}}\left(h+2b_{1y}\right)\right]-\frac{h^3}{12\mu_0}\frac{\partial p}{\partial y}\left[\frac{3}{h}\frac{(h+2b_{1y})(h+2b_{2y})}{b_{1y}+h+b_{2y}}-2\right]\right\}=-\frac{\partial h}{\partial t} \quad (9)$$

$$\frac{\partial^2\bar{P}}{\partial\theta^2}\left\{\frac{\bar{h}^{2+n}}{n}\left[\frac{3}{\bar{h}}\frac{(2B_{1x}+\bar{h})\,(2B_{2x}+\bar{h})}{B_{1x}+\bar{h}+B_{2x}}-2\right]\right\}+\frac{\partial\bar{P}}{\partial\theta}\left\{\frac{\bar{h}^{2+n}}{n}\left[\frac{3(2B_{1x}+\bar{h})}{\bar{h}\,(B_{1x}+\bar{h}+B_{2x})}-\frac{3(2B_{1x}+\bar{h})(2B_{2x}+\bar{h})}{\bar{h}^2(B_{1x}+\bar{h}+B_{2x})}+\frac{3(2B_{2x}+\bar{h})}{\bar{h}(B_{1x}+\bar{h}+B_{2x})}-\frac{3(2B_{1x}+\bar{h})(2B_{2x}+\bar{h})}{\bar{h}(B_{1x}+\bar{h}+B_{2x})^2}\right]\right\}+\left\{\left(\frac{n+2}{n}\right)\bar{h}^{n+1}\left(\frac{3(2B_{1x}+\bar{h})(2B_{2x}+\bar{h})}{\bar{h}^2(B_{1x}+\bar{h}+B_{2x})}-2\right)\right\}\frac{\partial\bar{h}}{\partial\theta}+\frac{\partial^2\bar{P}}{\partial\bar{y}^2}\left\{\bar{h}^{2+n}\left(\frac{D}{L}\right)^2\left(\frac{3(2B_{1y}+\bar{h})(2B_{2y}+\bar{h})}{\bar{h}(B_{1y}+\bar{h}+B_{2y})}-2\right)\right\}=6\left[\frac{\partial}{\partial\theta}\left\{\frac{\bar{h}(2B_{2x}+\bar{h})}{B_{1x}+\bar{h}+B_{2x}}\right\}\right]-12\frac{\partial\bar{h}}{\partial\tau} \quad (10)$$

Where the non-dimensional terms are obtained using

$$\bar{h}=\frac{h}{c},\theta=\frac{x}{r},\bar{y}=\frac{y}{L},\bar{P}=\frac{pc^{n+1}}{m\omega^n R^{n+1}},\mu_0=m\left(\frac{U}{h}\right)^{n-1},$$
$$v_x=u_{2x}-u_{1x},v_x=-u_b,$$
$$v_y=0,\quad u_{1x}=u_b,\quad u_{2x}=0,$$
$$v_{1y}=0,\quad B_{1x}=\frac{b_{1x}}{C},\ B_{1y}=\frac{b_{1y}}{C}$$

When n=1 (Newtonian fluid) and $B_{ix,iy}$=0 (no-slip condition), the revised Reynolds equation Eq. (10) reduces to the conventional Reynolds equation Eq. (11).

$$\frac{\partial}{\partial\theta}\left(\bar{h}^3\frac{\partial\bar{P}}{\partial\theta}\right)+\left(\frac{D}{L}\right)^2\frac{\partial}{\partial\bar{y}}\left(\bar{h}^3\frac{\partial\bar{P}}{\partial\bar{y}}\right)=6\frac{\partial\bar{h}}{\partial\theta}+12\frac{\partial\bar{h}}{\partial t} \quad (11)$$

The Finite Difference Method (FDM) is used to discretize the fluid film domain. Fig. 4 depicts the process of generating a finite difference mesh.

The steady-state pressure can be determined by applying the modified Reynolds equation, as stated in Eq. 10. To discretize the fluid film domain, the Finite Difference Method (FDM) is employed. By utilizing FDM, the fluid film domain is divided into discrete elements. Fig. 4 illustrates the process of generating a finite difference mesh. Through solving Eq. (10) and ensuring that the fluid domain satisfies the boundary requirements, the pressure at each node is obtained. To meet both boundary limitations and pressure convergence criterion, a Gauss-Seidel iterative technique with a consecutive over-relaxation scheme is utilized. The resulting steady-state pressures are then used to evaluate the force components accurately.

Furthermore, the assumed attitude angle 'ψ' is revised iteratively with a small increment until it converges to the desired value of 'ϕ'. A tolerance value of 10^{-4} is set to determine when the convergence is achieved. To calculate the load carrying capacity of the system, Simpson's rule is employed. This method allows for an accurate estimation of the load. After obtaining the dimensionless pressure and load in the three lobe bearings, steady-state parameters such as the Sommerfeld number, the friction variable, and the flow rate can be computed. In order to study the stability of the system, a nonlinear transient analysis is conducted. This analysis involves simulating the movement of the journal center. By analysing the system's response to transient conditions, valuable insights into its stability can be gained. Lastly, the mass parameter, which is dependent on the speed of the system, is determined using the equations of motion. These equations provide a means of quantifying the mass of the system and its influence on its dynamic behavior. The entire process utilized is outlined in the flowchart depicted in Fig. 5.

A Gauss-Seidel iterative technique with consecutive over-relaxation scheme is used to fulfil the boundary limitations and meet the pressure convergence criterion. The converging steady-state pressures are used to assess the force components. Resultant dimensionless load is given by Eq. (12)

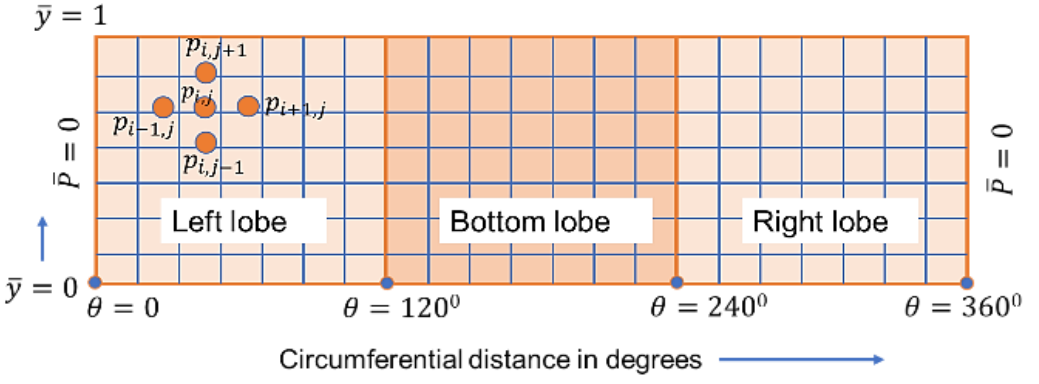

Fig. 4 Discretized mesh for three-lobe bearing.

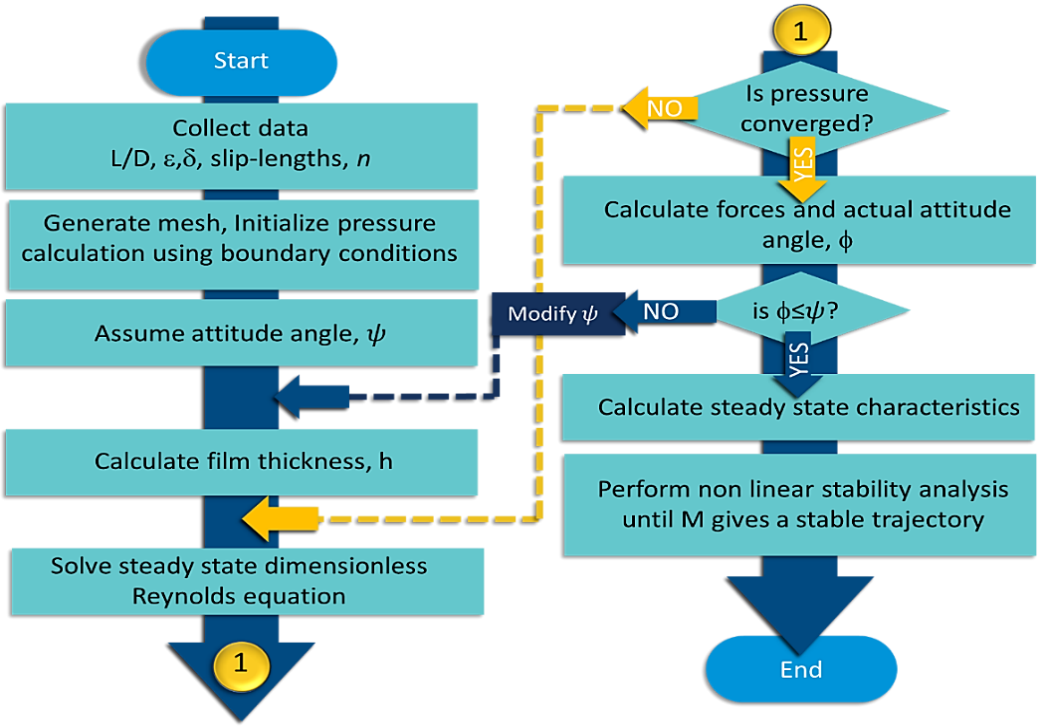

Fig. 5 Flowchart representing methodology implemented.

$$\bar{W} = \sqrt{\bar{W}_{\varepsilon}^2 + \bar{W}_{\phi}^2} \tag{12}$$

where

$$\bar{W}_{\varepsilon} = -\int_0^1 \int_0^{2\pi} \bar{P} \cos\theta \, \partial\theta \, \partial\bar{y} \tag{13}$$

$$\bar{W}_{\phi} = \int_0^1 \int_0^{2\pi} \bar{P} \sin\theta \, \partial\theta \, \partial\bar{y} \tag{14}$$

3. Stability Analysis

The three-lobe bearing's stability is investigated using a non-linear transient analysis that accounts for non-Newtonian fluid and wall-slip. By assigning the ellipticity ratio to 0.5 throughout, the non-Newtonian impact is created by applying a power law index ranging from 0.25 to 0.75 in 0.25 increments. The slip length is adjustable in 0.2 increments from 0 to 1. The proposed model can calculate the influence of slip length on both scenarios (B_{1x} or B_{2x}) at the same time. The analysis detailed here, however, only addresses the journal surface, that is, with one slip surface, B_{1x}, since it was discovered that the journal surface's lower slip length and greater power law index values have dominating impacts. Finally, $\bar{M}$ for ε is determined in 0.2 increments from 0.2 to 0.8.

3.1 Equations of motion

The equations of motion provided by Eq. (15) and (16) are utilised in a nonlinear time transient analysis for stability, referring to Fig. 6.

$$\bar{M}\bar{W}_o \left[\ddot{\varepsilon} - \varepsilon(\dot{\phi}^2)\right] = \bar{W}_{\varepsilon} + \bar{W}_o \cos\phi \tag{15}$$

$$\bar{M}\bar{W}_o \left[\varepsilon\ddot{\phi} + 2\dot{\varepsilon}(\dot{\phi})\right] = \bar{W}_{\phi} - \bar{W}_o \sin\phi \tag{16}$$

For solving the above two equations, Eq. (15) and Eq. (16), fourth-order Runge-Kutta technique is used to calculate the first and second-order ($\ddot{\varepsilon}$ and $\ddot{\phi}$) time derivatives. Then, using these time-varying values once more, Eq. (15) is applied to obtain $\bar{M}$. The stability of system is assessed using a journal center trajectory generated at a certain $\bar{M}$. The trajectory's value is then adjusted until the system obtains a trajectory that best describes its minimum stable state. The system repeats this operation with a fresh $\bar{M}$ until the critical state is reached,

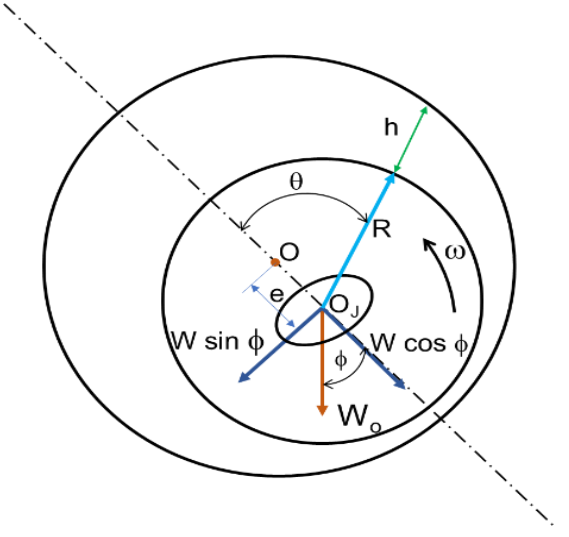

Fig. 6 Journal bearing used for steady state and dynamic analysis.

when it is stable below and unstable beyond that threshold. Such $\bar{M}$ values are documented, and a plot of stability is made.

3.2 Validation of the developed model

The mass parameter's performance versus com-parable measurements in the published literature is portrayed in Fig. 7.[36] The current model produces findings that are generally consistent with the existing literature.

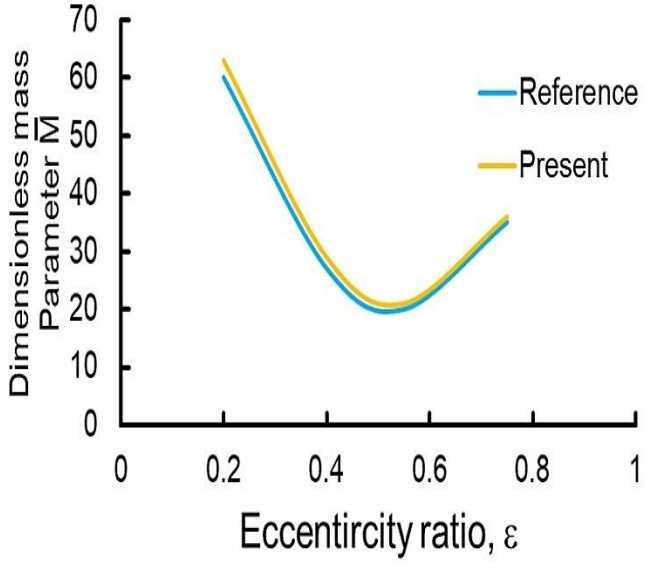

Fig. 7 Validation of stability with reference.[35]

4. Results and discussion

The present work is a continuation of our recently published research work.[37] It was discovered that the higher value of dimensionless pressure was developed for the bearing functioning with a lubricant having higher value PLI and lower value B_{ix}. When the slip was considered on the journal surface, the dimensionless pressure value was high. With wall-slip on the journal surface and non-Newtonian lubricant, the load-bearing capability was high and exceeded by about 15.38%.

The critical mass parameter is found at different eccentricity ratios for L/D = 1 and for various values of power law index, (usually less than unity, *i.e.*, for n < 1) with slip considered on the journal surface (B_{1x}). Upon reaching a limit cycle or transitioning from stable to unstable trajectory, the critical mass parameter corresponding to that eccentricity ratio is ascertained. Out of the possible combinations carried out, the details of the position of the journal centre for two groups serving as sample are plotted and are shown in Fig. 8 and Fig. 9. The mass parameters acquired for various three lobe journal bearing designs are given in Table 1 to examine the bearing system's stability. As was done by Akers *et al.*,[38] trajectories are noted following each full circle of the shaft in order to calculate the whirl ratio at the incipient whirl point. The journal's trajectory plots illustrate the journal's movement around the bearing center over time. These plots are an effective tool for analyzing the transient stability characteristics of the system. The trajectory plots typically consist of a circular or elliptical path representing the journal's movement. The center of the plot represents the bearing center, while the size and shape of the trajectory indicate the stability of the system. A stable system will often exhibit a small circular or elliptical trajectory, indicating smooth and consistent journal motion around the bearing center. On the other hand, an unstable system may show larger and irregular trajectories, suggesting the presence of vibrations or other instabilities.

Figures 8a-8d to Figs. 9a-9d aids in understanding the system stability for various journal parameter combinations. These diagrams illustrate the motion trajectory of the journal over time, showcasing the characteristics of the journal centre's location. These figures represent the marginally stable circumstances, where the journal approaches equilibrium by establishing a limit cycle. By observing the journal trajectories, it becomes evident that as the PLI increases, the mass parameter $\bar{M}$ also increases for a given B_{1x} and ε. Consequently, the limit cycle gradually shifts towards the center of the clearance circle, indicating higher stabilities.

For a particular slip length and pre-load factor, an increase in stability area by an average of 21% is observed. For a given L/D ratio, the value of $\bar{M}$ offers a specific stable margin for every combination of preload factor and slip length. This indicates the upper limit of the critical mass range that may cause instability in the three-lobe journal-bearing system. It can be concluded that a three-lobe journal bearing system with lower slip length=0.2 and higher *n* (0.95) offers better stability than operating with higher slip length=0.6 and higher *n*.

For a particular slip length and pre-load factor, an increase in stability area by an average of 21% is observed. For a given L/D ratio, the value of $\bar{M}$ offers a specific stable margin for every combination of preload factor and slip length. This indicates the upper limit of the critical mass range that may cause instability in the three-lobe journal-bearing system. It can be concluded that a three-lobe journal bearing system with lower slip length=0.2 and higher *n* (0.95) offers better stability than operating with higher slip length=0.6 and higher *n*.

The stability curves in Figs. 9(a) and (b) are derived by graphing the mass parameters against the eccentricity ratio for varied slip lengths and with an ellipticity ratio of δ=0.5. Fig. 10(a) represents the case when *n*=0.75 and Fig. 10(b) when *n*=0.5

Table 1. Mass parameter obtained for journal bearing configurations.

	Combination	B_{1x}	δ	n	L/D	e	$\bar{M}$
Group-1	C1	0.2	0.5	0.25	1	0.2	7.31
	C2					0.4	7.36
	C3					0.6	9.34
	C4					0.8	36.0
Group-2	C1	0.2	0.5	0.50	1	0.2	9.15
	C2					0.4	10.3
	C3					0.6	14.0
	C4					0.8	37.0
Group-3	C1	0.2	0.5	0.75	1	0.2	14.0
	C2					0.4	14.0
	C3					0.6	20.0
	C4					0.8	40.0
Group-4	C1	0.2	0.5	0.95	1	0.2	17.54
	C2					0.4	18.65
	C3					0.6	24.8
	C4					0.8	58.0
Group-5	C1	0.6	0.5	0.25	1	0.2	6.04
	C2					0.4	5.90
	C3					0.6	7.20
	C4					0.8	35.6
Group-6	C1	0.6	0.5	0.50	1	0.2	7.52
	C2					0.4	8.36
	C3					0.6	10.5
	C4					0.8	40.0
Group-7	C1	0.6	0.5	0.75	1	0.2	10.67
	C2					0.4	11.45
	C3					0.6	19.40
	C4					0.8	42.00
Group-8	C1	0.6	0.5	0.95	1	0.2	14.74
	C2					0.4	15.10
	C3					0.6	23.00
	C4					0.8	45.24

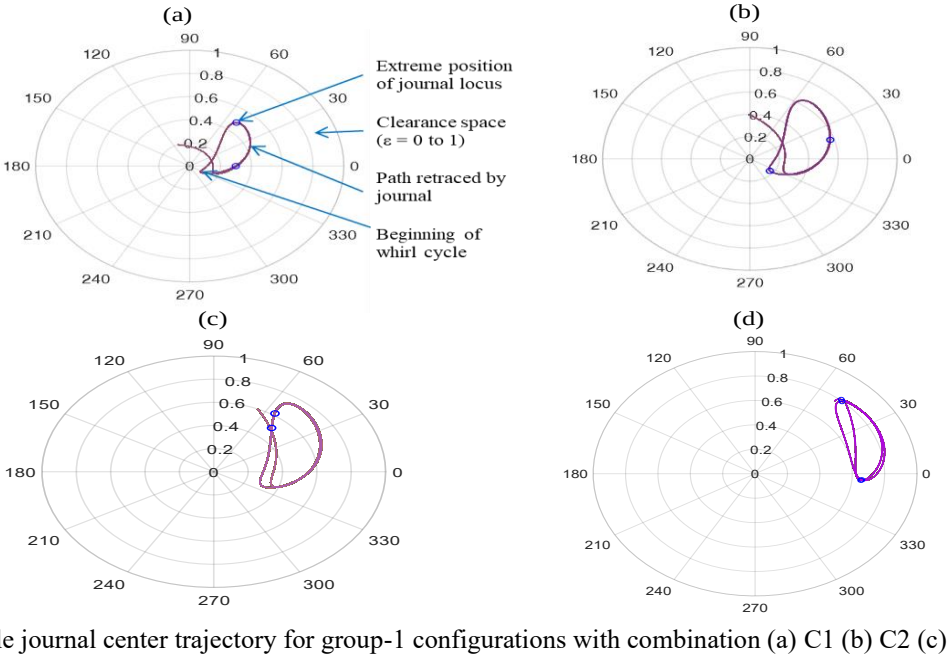

Fig. 8 Sample journal center trajectory for group-1 configurations with combination (a) C1 (b) C2 (c) C3 (d) C4.

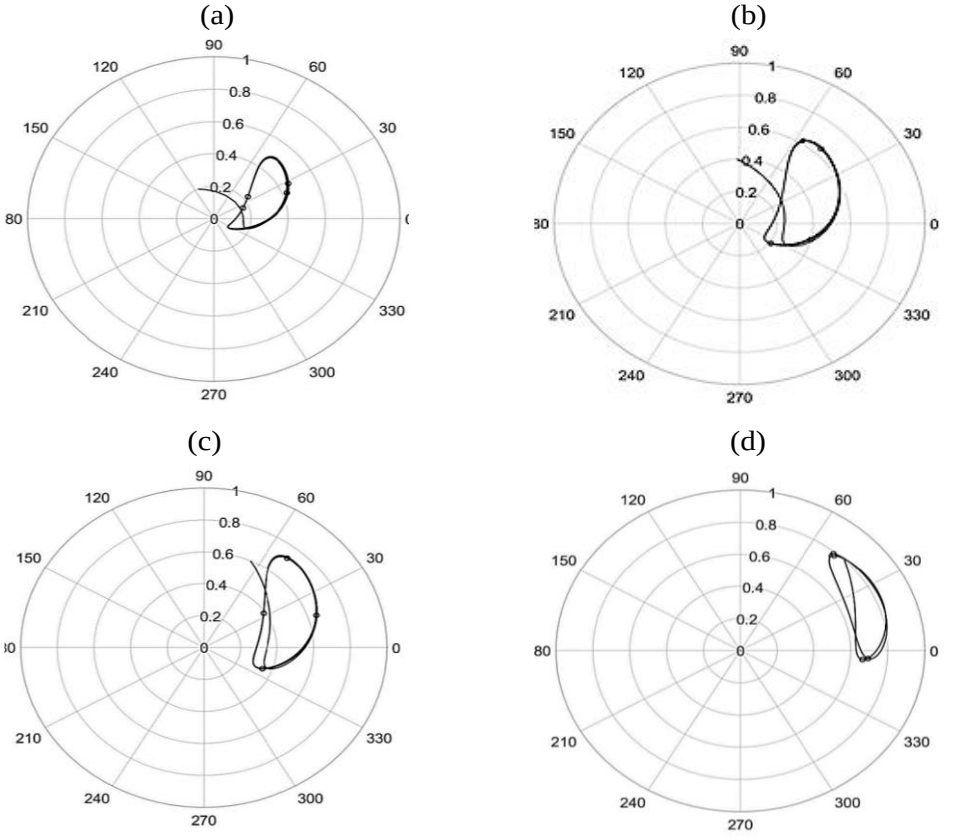

Fig. 9 Sample journal center trajectory for group-5 configurations with combination (a) C1 (b) C2 (c) C3 (d) C4.

With rising eccentricity ratios and lowering power law index, the whirl ratio of three lobe bearing, as portrayed in Fig. 11, decreases. The eccentricity ratio of 0.8 results in the lowest whirl ratio for $n = 0.75$. This variation may be observed for all power law index levels ranging from 0.25 to 0.75. The three-lobe bearing should have a higher power law index and a greater eccentricity ratio to function with the least amount of whirling.

Figure 12 depicts the fluctuation of the dimensionless mass parameter, $\bar{M}$, for separate n values for $B_{1x} = 0.2$. The results show that a greater stability zone is achieved with a lower L/D ratio; however, as the ratio rises, the stability decreases. Comparing the stability with $\bar{M}$=17 at L/D=1.5 to that of $\bar{M}$=21 at L/D=1, the highest mass parameter indicates a greater stability feature.

4.1 Sensitivity analysis on key parameters

A sensitivity analysis was conducted to investigate the

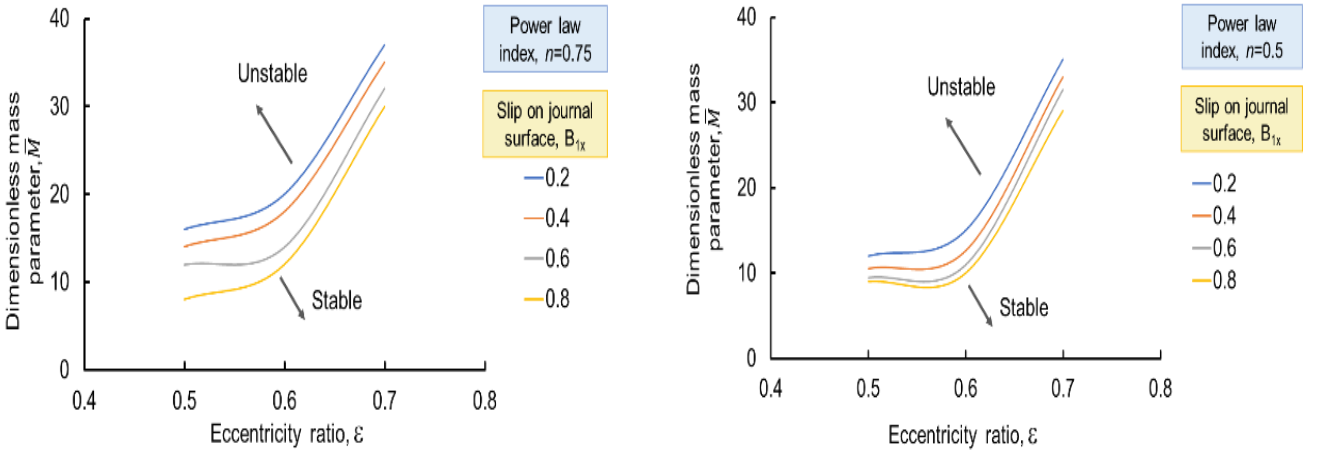

Fig. 10 Variation of mass parameter with slip length for (a) n=0.75 (b) n=0.5.

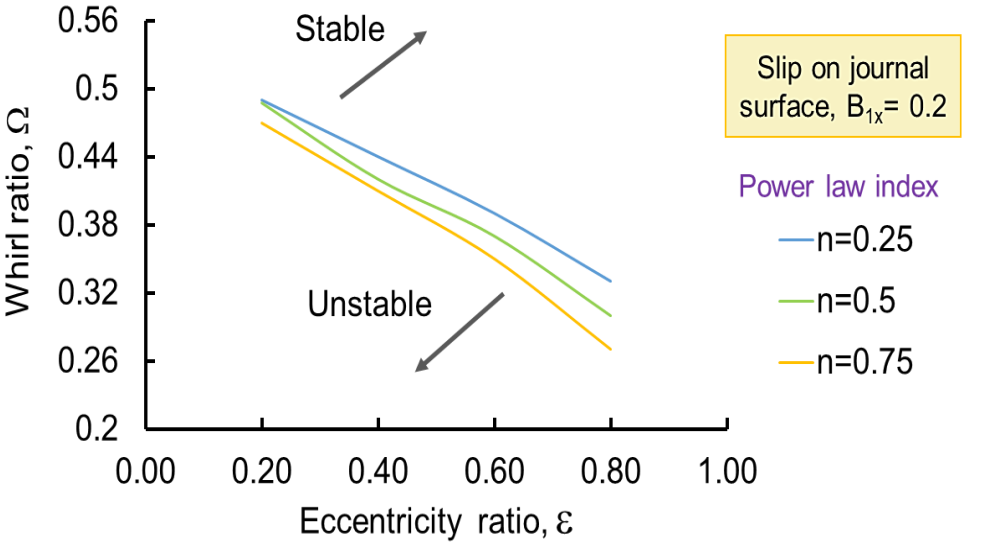

Fig. 11 Whirl ratio for varying power law index for slip-length of B_{1x}=0.2.

individual impact of key parameters, such as PLI and slip lengths, on the stability of the bearing. In order to determine the sensitivity of PLI, the slip length was held at a constant value while the PLI values were varied from 0.25 to 0.95 with an increment of 0.25. The mass parameter, which indicates a marginally stable condition of the journal, was recorded, and presented in Table 2. Mass parameter obtained for journal bearing configurations These readings were obtained under the conditions of ε=0.4, L/D=1, and δ=0.5. A graph was plotted using the tabulated values and is shown in Fig. 12.

Table 2. Sensitivity analysis of slip lengths on the bearing system

ε	B_{1x}	PLI	$\bar{M}$
0.4	0	0.25	9.1
		0.50	12.6
		0.75	18.02
		0.95	24.03

The sensitivity analysis revealed a direct relationship between PLI and $\bar{M}$ indicating that the stability of the bearing is influenced by the PLI for the given eccentricity ratio and slip length. Additionally, the use of Pseudoplastic fluids as lubricants introduces additives that fill the gaps between the sliding surfaces, enhancing the damping effect and ultimately increasing stability.

Table 3. Sensitivity analysis of PLI on the bearing system.

PLI	ε	B_{1x}	$\bar{M}$
1	0.4	0	26.6
		0.2	20.12
		0.4	18.27
		0.8	14.4

Similarly, to examine the sensitivity of wall slip on the bearing, the PLI was set at a fixed value while the slip lengths were varied from 0.2 to 0.8 with an increment of 0.2. The mass parameter indicating a marginally stable condition of the journal was recorded and presented in Table 3. These readings were obtained under the conditions of ε=0.4, L/D=1, and δ=0.5. A graph was plotted using the tabulated values and is shown in same Fig. 12. The analysis revealed that as the slip length increases, the stability of the bearing decreases for the selected eccentricity ratio and PLI. This is due to the higher tendency of the bearing to slip with increasing slip length, leading to a decrease in stability.

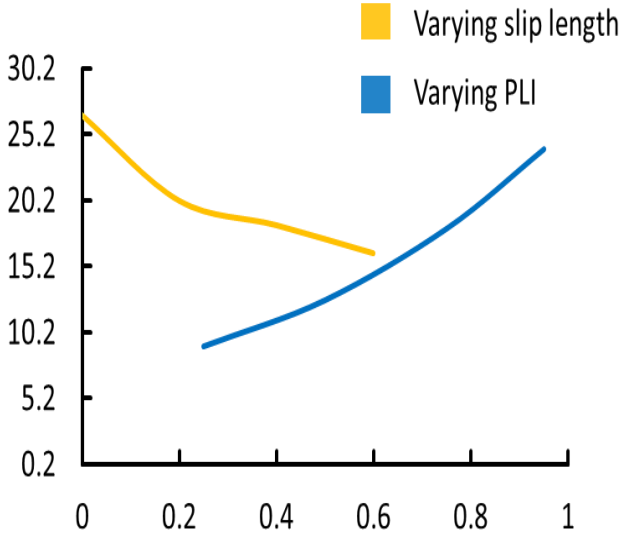

Fig. 12 Sensitivity analysis of PLI and slip length on the three-lobe bearing.

4.2 Comparative analysis between the results obtained with slip and no-slip conditions

The analysis of the journal trajectories aimed to compare the

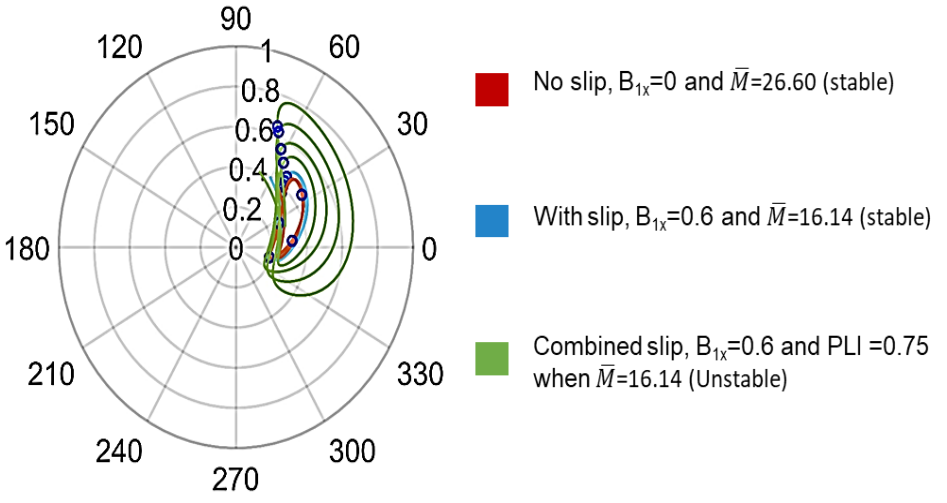

Fig. 13 comparison of stability with slip and no slip conditions for ε=0.4, L/D=1, δ=0.5.

outcomes obtained under slip and no-slip conditions. For a specific set of parameters, namely ε=0.4, L/D=1, and δ=0.5 by altering the value of M, the marginal stable limit cycle was determined for both the no-slip condition (B1x=0) and the wall-slip condition (B1x=0.6). The bearing was found to be marginally stable at M=26.60 and M=16.14 for the slip and no-slip cases, respectively as depicted in Fig. 13.

In order to examine whether the bearing remains stable even when subjected to the combined effect of wall-slip and a pseudoplastic lubricant, a PLI of 0.75 was introduced simultaneously with the parameters ε=0.4, L/D=1, δ=0.5, and B_{1x}=0.6 for M=16.14. It was observed that the addition of slip length caused the journal to become unstable at M=16.14, which was initially stable. This comparative study revealed that the parameters like wall-slip and PLI effects have a significant impact on the performance of the bearing. This instability can be attributed to the increase in operational speed for a specific mass parameter. The increase in speed resulted in an unstable state for the system. The change in the PLI played a role in this instability by increasing the load carrying capacity. As a consequence, the system's speed also increased, ultimately leading to its instability.

5. Conclusions

The study focused on improving the stability of a journal-bearing system. This system is designed with three lobes to provide a more stable support for the rotating shaft. In addition to the three-lobe design, the slip length of the bearing system also played a crucial role in enhancing stability. In this study, a smaller slip length of B1x=0.2 had a greater impact. Moreover, the type of fluid used in the bearing system had impact on its stability. Non-Newtonian fluids, like the one utilized in this investigation, possess unique flow properties that can enhance stability. The utilization of a power law index (PLI) of n=0.95 for the fluid helps minimize fluctuations and disruptions within the bearing system. The study findings demonstrated a noteworthy enhancement in stability through the implementation of these adjustments. On average, there was a 21% increase in the stability area, which refers to the range of operating conditions where the bearing system can maintain consistent performance. Consequently, this translates to improved reliability and efficiency across a broader spectrum of conditions, thereby reducing the risk of potential failures or malfunctions.

The PLI serves as an indicator of a bearing's capacity to deliver stable and efficient operation. A higher PLI corresponds to greater stability and enhanced performance, resulting in reduced whirling effects. Additionally, slip-length plays a crucial role in mitigating whirling phenomena. By reducing the slip-length, unsteady motion and vibration are minimized, contributing to a more stable operation with less whirling.

Furthermore, it should be noted that the L/D ratio of a three-lobe journal-bearing system affects its stability, as highlighted by the non-dimensional mass parameter. As the L/D ratio increases, so too does instability within the bearing system. This implies that higher L/D ratios are associated with elevated risks of unsteady motion and vibration, leading to more pronounced whirling effects.

6. Scope for future exploration

In order to further enhance the current research work, there are several potential future avenues that can be explored. The research conducted so far has been under isothermal settings, which are not commonly encountered in practical scenarios. Therefore, it would be valuable to investigate the effects of

heat on lubricant viscosity. Another area of improvement lies in the cavitation region. By incorporating more accurate models for cavitation and reformation boundary conditions, we can enhance our understanding of this phenomenon.

Conflict of Interest

There is no conflict of interest.

Supporting Information

Not applicable.

Nomenclature

b_{ix}	Slip length along x direction of i[th] surface (m), $B_{ix} = \frac{b_{ix}}{C}$
b_{iy}	Slip length along y direction of i[th] surface (m), $B_{iy} = \frac{b_{iy}}{C}$
C	Lobe clearance, m
C_m	Minor clearance, m
D	Diameter of journal, m
e	Eccentricity, m
h	Thickness of fluid film, m, $\bar{h} = \frac{h}{c}$
L	Length of journal, m
m	Pseudoplastic viscosity constant, m = $(U/C)^{n-1}$, Ns/m^2
M	Mass of rotor, kg
$\bar{M}$	Mass parameter, $\bar{M} = \frac{MC\omega^2}{W_o}$
n	Power law index
p	Pressure (N/m^2), $\bar{P} = \frac{pC^{n+1}}{m\omega^n R^{n+1}}$
R+C	Lobe Radius, m
R	Journal Radius, m
t	Time, s
U	Journal Velocity, m/s
U_b	Boundary velocity, m/s
W	Load carrying capacity, N, $\bar{W} = \frac{WC^{n+1}}{m\omega^n R^{n+2} L}$
W_o	Steady state load carrying capacity N, $\bar{W} = \frac{W_o C^{n+1}}{m\omega^n R^{n+2} L}$
W_c	Unidirectional constant load, $\bar{W}_c = \frac{W_c C^2}{m\omega^n R^{n+2} L}$
y	Coordinate along the bearing axis, $\bar{y} = \frac{y}{L/2}$
z	Bearing axial coordinate
x,y,z	Coordinates
$\delta = \frac{d}{C}$	Ellipticity ratio
$\varepsilon = \frac{e}{C}$	Eccentricity ratio
θ	Circumferential coordinate $= \frac{x}{r}$
θ_s, θ_c	Angular coordinates when film starts and cavitates
ϕ	Bearing attitude angle, rad
ϕ_B, ϕ_L, ϕ_R	Bottom, left and right lobe attitude angle, rad
ω	Angular velocity of the journal, rad/sec
ω_p	Whirl angular velocity, rad/sec
ψ	Assumed attitude angle, rad
τ	Time in dimensionless form, $\tau = \omega t$
Ω	Whirl ratio, $\Omega = \frac{\omega_p}{\omega}$

References

[1] Y. Zhu, S. Granick, Rate-dependent slip of Newtonian liquid at smooth surfaces, *Physical Review Letters*, 2001, **87**, 096105, doi: 10.1103/Phys Rev Lett 87.096105.

[2] Y. Zhu, S. Granick, Limits of the hydrodynamic No-slip boundary condition, *Physical Review Letters*, 2002, **88**, 106102, doi: 10.1103/physrevlett.88.106102.

[3] J. H. Choo, R. P. Glovnea, A. K. Forrest, H. A. Spikes, A low friction bearing based on liquid slip at the wall, *Journal of Tribology*, 2007, **129**, 611-620, doi: 10.1115/1.2736704.

[4] M. Tauviqirrahman, R. Ismail, J. Jamari and D. J. Schipper, Wall slip effects in a lubricated MEMS, *International Journal of Energy Machinery*, 2011, **4**, 13-22.

[5] J.-R. Lin, P.-J. Li, T.-C. Hung, L.-J. Liang, Nonlinear stability boundary of journal bearing systems operating with non-Newtonian couple stress fluids, *Tribology International*, 2014, **71**, 114-119, doi: 10.1016/j.triboint.2013.10.010.

[6] M. Kane, B. Bou-Said, A study of roughness and non-Newtonian effects in lubricated contacts, *Journal of Tribology*, 2005, **127**, 575-581, doi: 10.1115/1.1866169.

[7] C. Aiumpornsin, M. Mongkolwongrojn, Influence of Surface Roughness on Elastohydrodynamic Journal Bearings with Non-Newtonian Lubricants. In: Luo, J., Meng, Y., Shao, T., Zhao, Q. (eds) Advanced Tribology. Springer, Berlin, Heidelberg, 2010, 50-51, doi: 10.1007/978-3-642-03653-8_20

[8] H.-L. Chiang, J.-R. Lin, C.-H. Hsu, Y.-P. Chang, Linear stability analysis of a rough short journal bearing lubricated with non-Newtonian fluids, *Tribology Letters*, 2004, **17**, 867-877, doi: 10.1007/s11249-004-8095-8.

[9] M. M. Khonsari, D. E. Brewe, On the performance of finite journal bearings lubricated with micropolar fluids, *Tribology Transactions*, 1989, **32**, 155-160, doi: 10.1080/10402008908981874.

[10] A. Nessil, S. Larbi, H. Belhaneche, M. Malki, Journal bearings lubrication aspect analysis using non-Newtonian fluids, *Advances in Tribology*, 2013, **2013**, 1-9, doi: 10.1155/2013/212568.

[11] Z. S. Safar, Journal bearings operating with non-Newtonian lubricant films, *Wear*, 1979, **53**, 95-100, doi: 10.1016/0043-1648(79)90220-5.

[12] F. Rahmani, R. K. Pandey, J. K. Dutt, Influence of elliptic bore and non-Newtonian rheology of lubricant on the performance and stability of journal bearing, *Procedia Technology*, 2016, **23**, 28-35, doi: 10.1016/j.protcy.2016.03.069.

[13] W. A. Crosby, B. Chetti, The static and dynamic characteristics of a two-lobe journal bearing lubricated with couple-stress fluid, *Tribology Transactions*, 2009, **52**, 262-268, doi: 10.1080/10402000802527773.

[14] K. Raghunandana, B. C. Majumdar, Stability of journal bearing systems using non-Newtonian lubricants: a non-linear transient analysis, *Tribology International*, 1999, **32**, 179-184, doi: 10.1016/s0301-679x(99)00027-4.
[15] B. Chetti, W. A. Crosby, Preload effects on the static characteristics of three-lobe journal bearings lubricated with a couple stress fluid, *Industrial Lubrication and Tribology*, 2019, **71**, 1136-1143, doi: 10.1108/ilt-12-2018-0435.
[16] B. J. Das, L. Roy, Analysis and comparison of steady-state performance characteristics of two-axial groove and multilobe hydrodynamic bearings lubricated with non-Newtonian fluids, *Proceedings of the Institution of Mechanical Engineers, Part J: Journal of Engineering Tribology*, 2018, **232**, 12, 1581-1596, doi: 10.1177/1350650118758087.
[17] T. V. V. L. N. Rao, A. M. A. Rani, T. Nagarajan, F. M. Hashim, Analysis of slider and journal bearing using partially textured slip surface, *Tribology International*, 2012, **56**, 121-128, doi: 10.1016/j.triboint.2012.06.010.
[18] G. J. Ma, C. W. Wu, P. Zhou, Wall slip and hydrodynamics of two-dimensional journal bearing, *Tribology International*, 2007, **40**, 1056-1066, doi: 10.1016/j.triboint.2006.10.003.
[19] F. Aurelian, M. Patrick, H. Mohamed, Wall slip effects in (elasto) hydrodynamic journal bearings, *Tribology International*, 2011, **44**, 868-877, doi: 10.1016/j.triboint.2011.03.003.
[20] C.-Y. Chen, Q.-D. Chen, W.-L. Li, Characteristics of journal bearings with anisotropic slip, *Tribology International*, 2013, **61**, 144-155, doi: 10.1016/j.triboint.2012.12.017.
[21] A. E. Fortier, R. F. Salant, Numerical analysis of a journal bearing with a heterogeneous slip/No-slip surface, *Journal of Tribology*, 2005, **127**, 820-825, doi: 10.1115/1.2033897.
[22] G. Ma, C. Wu, P. Zhou, Hydrodynamics of slip wedge and optimization of surface slip property, *Science in China Series G: Physics, Mechanics and Astronomy*, 2007, **50**, 321-330, doi: 10.1007/s11433-007-0034-x.
[23] Q. Lin, Z. Wei, Y. Tang, Numerical study on shear flow in sliding bearing with partial slip surface, *Procedia CIRP*, 2012, **3**, 197-202, doi: 10.1016/j.procir.2012.07.035.
[24] M. J. Walsh, Riblets,1990, 203-261, M. J. Walsh, in Viscous Drag Reduction in Boundary Layers, D. M. Bushnell, J. N. Hefner, Eds., American Institute of Aeronautics and Astronautics, 1090, **123**, 203-261.
[25] B. Bhushan, Y. Wang, A. Maali, Boundary Slip Study on Hydrophilic, Hydrophobic, and Superhydrophobic Surfaces with Dynamic Atomic Force Microscopy, *Langmuir*, 2009, **25**, 8117-8121, doi: 10.1021/la900612s.
[26] H. Spikes, S. Granick, Equation for slip of simple liquids at smooth solid surfaces**,** *Langmuir***,** 2003, **19**, 5065-5071, doi: 10.1021/la034123j.
[27] M. Tauviqirrahman, J. Jamari, S. Susilowati, C. Pujiastuti, B. Setiyana, A. H. Pasaribu, M. I. Ammarullah, Performance comparison of Newtonian and non-Newtonian fluid on a heterogeneous slip/No-slip journal bearing system based on CFD-FSI method, *Fluids*, 2022, **7**, 225, doi: 10.3390/fluids7070225.
[28] M. Arif, D. K. Shukla, S. Kango, N. Sharma, Implication of surface texture and slip on hydrodynamic fluid film bearings: a comprehensive survey, *Tribology Online*, 2020, **15**, 265-282, doi: 10.2474/trol.15.265.
[29] S. Muhammad Bilal, N. Zeb Khan, R. Nisar, FEM simulations to analyze flow and thermal characteristics of carreau non-Newtonian fluid in a square cavity, *International Journal of Emerging Multidisciplinaries*: *Mathematics*, 2023, **2**, 3, doi: 10.54938/ijemdm.2023.02.1.146.
[30] S. Bilal, N. Z. Khan, S. M. Eldin, FEM analysis of the impact of surface undulations on the natural convective flow of viscous fluid in a permeable trapezoidal enclosure, *Frontiers in Physics*, 2023, **11**, 1153645, doi: 10.3389/fphy.2023.1153645.
[31] Q. Lin, Z. Wei, N. Wang, W. Chen, Effect of large-area texture/slip surface on journal bearing considering cavitation, *Industrial Lubrication and Tribology*, 2015, **67**, 216-226, doi: 10.1108/ilt-05-2013-0055.
[32] M. M. Mohseni, F. Rashidi, Axial annular flow of a Giesekus fluid with wall slip above the critical shear stress, *Journal of Non-Newtonian Fluid Mechanics*, 2015, **223**, 20-27, doi: 10.1016/j.jnnfm.2015.05.004.
[33] M. Moayed Mohseni, G. Tissot, M. Badawi, Effects of wall slip on convective heat transfers of giesekus fluid in microannulus, *Journal of Heat Transfer*, 2020, **142**, 082503, doi: 10.1115/1.4046642.
[34] M. M. Mohseni, G. Tissot, M. Badawi, Forced convection heat transfer of Giesekus fluid with wall slip above the critical shear stress in pipes, *International Journal of Heat and Fluid Flow*, 2018, **71**, 442-450, doi: 10.1016/j.ijheatfluidflow.2018.05.005.
[35] W.-L. Li, H.-M. Chu, M.-D. Chen, The partially wetted bearing—extended Reynolds equation, *Tribology International*, 2006, **39**, 1428-1435, doi: 10.1016/j.triboint.2006.01.009.
[36] N. Abdul-Wahed, D. Nicolas, M. T. Pascal, Stability and unbalance response of large turbine bearings, *Journal of Lubrication Technology*, 1982, **104**, 66-75, doi: 10.1115/1.3253166.
[37] A. M. Ambekar, Effect of wall-slip and non-newtonian fluid on the steady-state performance of a three-lobe bearing**,** *Journal of Mines, Metals & Fuels*, 2023, **71**, 208-216, doi: 10.18311/JMMF/2023/33383.
[38] A. Akers, S. Michaelson, A. Cameron, Stability contours for a whirling finite journal bearing, *Journal of Lubrication Technology*, 1971, **93**, 177-183, doi: 10.1115/1.3451510.